JOURNAL OF CATALYSIS 149, 149–158 (1994)

Promotion of CO and CO_2 Hydrogenation over Rh by Metal Oxides: The Influence of Oxide Lewis Acidity and Reducibility

A. Boffa,* C. Lin,† A. T. Bell,† and G. A. Somorjai*

*Materials Sciences Division, Lawrence Berkeley Laboratory, Berkeley, California 94720; and Departments of *Chemistry and †Chemical Engineering, University of California, Berkeley, California 94720*

Received October 18, 1993; revised May 10, 1994

An investigation has been carried out of CO and CO_2 hydrogenation to methane over a Rh foil decorated with submonolayer quantities of AlO_x, TiO_x, VO_x, FeO_x, ZrO_x, NbO_x, TaO_x, and WO_x. The rate of methane formation was measured at 1 atm and the state of the working catalyst was characterized by XPS immediately after reaction. With the exception of AlO_x, each of the oxides was found to enhance the rate of CO methanation relative to that observed over unpromoted Rh. The maximum degree of rate enhancement occurs at an oxide coverage of approximately half a monolayer. AlO_x retards the formation of methane in direct proportion to the oxide coverage. FeO_x behaves in a manner identical to that of AlO_x in the case of CO_2 hydrogenation, whereas all of the other oxides studied produce a maximum degree of methanation rate enhancement at an oxide coverage of half a monolayer. The enhancement of CO and CO_2 hydrogenation is attributed to the formation of Lewis acid–base complexes between the oxygen end of adsorbed CO (or H_2CO formed during the reaction) and anionic vacancies present at the edge of the oxide–metal boundary. The degree of enhancement of CO and CO_2 hydrogenation is found to increase with the average oxidation state of the metal in the oxide overlayer. This trend is attributed to the direct relationship between Lewis acidity of an oxide and the oxidation state of the metal in the oxide. The degree of reduction of a given oxide is found to be higher during CO_2 hydrogenation than CO hydrogenation. © 1994 Academic Press, Inc.

INTRODUCTION

The rate of hydrogenation of polar molecules (e.g., CO, CO_2, RCHO, NO) over transition metal catalyst surfaces can be dramatically increased by decoration of the metal surfaces with small amounts of transition metal oxides (1–5). For example, in the case of Rh, the oxides of Ti (4, 6), V (7), Mn (8), Zr (9), Nb (10, 11), Mo (12), and Hf (13) have been found to enhance the rates of CO and CO_2 hydrogenation to methane and other hydrocarbons. Similar effects have been observed for TiO_x deposited on Ni, Pd, Pt, and Ru (1–5).

The origin of the observed effects of metal oxides on the catalytic properties of transition metals has been the subject of considerable discussion in the literature. In the earliest attempts to provide an explanation, Schwab (14) and Solymosi (15) proposed that the metal oxide altered the electronic properties of the metal. While this hypothesis was soundly based on the principles of metal/semiconductor interfaces, subsequent experimental data revealed no evidence for a change in the bulk electronic properties of the metal due to the presence of metal/metal oxide contacts. This led to the proposal, first articulated by Burch and Flambard (16), that highly active sites occur in the metal/metal oxide interfacial region. These sites were envisioned to be cations or anionic vacancies present at the edge of the metal oxide moieties. The activation of C=O bonds was proposed to occur via interaction of the oxygen end of a carbonyl group with the cation site, thereby inducing activation of the C=O bond to hydrogenation. In later work, Sachtler and co-workers (8, 17) suggested that the nature of the interaction between the carbonyl group and the exposed cation at the edge of the oxide moiety might be similar to that of Lewis acid–base complexes formed in solution between carbonyl ligands in metallocarbonyl complexes and Lewis acids such as $AlCl_3$.

The majority of previous studies of metal oxide promotion of CO and CO_2 hydrogenation have been conducted using metals dispersed on a high surface area support. While such investigations are effective in revealing the influence of support composition on the rate of CO and CO_2 hydrogenation, there are significant difficulties in determining unambiguously the coverage of the metal surface by metal oxide moieties derived from the support. Several recent investigations have shown that the effects of metal oxide deposits on the catalytic properties of metals can be studied much more effectively using planar model systems consisting of a metal foil or single crystal surface decorated with submonolayer quantities of the oxide (18–28). Such systems enable control of the oxide coverage, and characterization of the oxide composition by various surface analytical techniques.

This study was undertaken to investigate the influence of oxide composition on the rates of CO and CO_2 hydrogenation over Rh. To this end, a Rh foil was decorated

0021-9517/94 $6.00

with submonolayer quantities of AlO_x, TiO_x, VO_x, FeO_x, ZrO_x, NbO_x, TaO_x, and WO_x. The catalyst surface was characterized by both Auger electron spectroscopy (AES) and X-ray photoelectron spectroscopy (XPS) to determine the oxide coverage and composition, respectively. Studies of the rates of CO and CO_2 hydrogenation were then carried out for a range of metal oxide coverages. The results of this study show that the effectiveness of different oxides in promoting CO and CO_2 hydrogenation correlates with the oxidation state of the oxide, with higher oxidation state, in general, resulting in a higher degree of enhancement in the reaction rate. It is shown as well that the oxidation state of a given metal oxide can strongly depend on the nature of the reaction.

EXPERIMENTAL

Sample preparation and characterization and subsequent reaction studies were performed in a Varian UHV chamber equipped with a cylindrical mirror analyzer for Auger electron spectroscopy, an EAI quadrupole mass spectrometer, and an atmospheric-pressure isolation cell (26, 28). The chamber is evacuated by an oil diffusion pump and a titanium sublimation pump to achieve a base pressure of 1×10^{-9} Torr. The sample, 1 cm^2 Rh polycrystalline foil, 0.002 in. thick, is attached to a manipulator by 0.02-in. gold wires spot welded to the foil. An S-type thermocouple is spot welded to the foil for temperature measurement. Prior to the initiation of a reaction, the foil is cleaned by high temperature annealing and sputtering to remove boron and sulfur contamination.

Metals were deposited on the Rh surface by using an evaporator. The filaments in the evaporator consisted of either a 0.02-in. or a 0.04-in. wire of the metal to be deposited in the case of W, Ta, Nb, and Zr or a 0.005-in. to 0.02-in. wire of the metal to be deposited wound around a 0.04-in. W wire in the case of Ti, V, Fe, and Al. Currents of between 20 and 40 A were necessary to give a deposition rate of approximately 1.0 ml/min. A back pressure of 2×10^{-7} Torr of oxygen was present during evaporation in order to reduce carbon contamination. After metal deposition, the surface was oxidized in 1×10^{-6} Torr of O_2 at 623 K for 5 min. To remove oxygen adsorbed on the exposed Rh surface, 2×10^{-7} Torr of CO was admitted into the chamber for 20 s, and the sample was then flashed to 673 K. The bare Rh surface was given the same gas exposures before reaction to eliminate the possibility of ascribing rate enhancements to pretreatment effects. When necessary, the deposited oxide was removed by Ar^+ ion sputtering, after which the sample was annealed to remove any defects.

The coverage of the metal oxide was determined by the extent of attenuation in the Rh (302 eV) AES signal observed following deposition of the oxide. For each of the oxides investigated it was observed that for surface coverages of up to 1 ML the Rh AES intensity falls off linearly. Slight deviations from linearity were noted only for deposition times close to those required to achieve monolayer coverage. Based on these observations it was concluded that the deposited oxides grow two-dimensionally up to a coverage of >0.9 ML, whereafter some three-dimensional growth occurs.

To perform a reaction, the sample was enclosed in a high-pressure cell connected to a gas recirculation loop. The total volume of the reactor and recycle loop is 120 cm^3. H_2, CO, or CO_2, purified through a trap maintained at 150 K, were introduced into the loop and argon was added when necessary to give a total pressure of 760 Torr. A metal bellows pump was used to recirculate the gases at a flow rate of approximately 100 cm^3/min. The accumulation of reaction products in the loop was monitored with an HP 5890A gas chromatograph equipped with an FID. A stainless steel 10-ft × $\frac{1}{8}$-in. column packed with 80/120 Carbopak B coated with 3% SP1500 was used for product separation. All reactions were run at CO and CO_2 conversions of less than 5%. After reaction, approximately 10 min were required to return the UHV chamber to its base pressure.

A PHI ESCA 5300 system was used for characterization metal oxide deposits on Rh by X-ray photoelectron spectroscopy (XPS). This system is equipped with Mg and Al anode X-ray sources, a differentially pumped He and Ar ion gun, a hemispherical analyzer, and a sample preparation cell. For XPS, the Mg anode (1253.5 eV) was used, and the hemispherical analyzer was operated at a 8.75 eV pass energy. Before analysis, catalyst samples were prepared in a chamber attached directly to the main vacuum chamber. The base pressure in the preparation chamber was 1×10^{-9} Torr. A transfer rod was used to move the sample between the preparation chamber and the analysis chamber. Following preparation and initial characterization, the sample could be transferred using a transfer rod to an atmospheric-pressure isolation cell, where the sample was then exposed to reactants at elevated temperature. After treatment under atmospheric conditions, the sample was cooled to below 473 K at which point the isolation cell was evacuated to less than 1×10^{-6} Torr with a turbomolecular pump in approximately 3 min. The sample was then transferred directly to the analysis chamber under vacuum.

RESULTS

The effects of metal oxide deposits on the rate of methane formation from CO and CO_2 over Rh are shown in Figs. 1 and 2, respectively. The relative rate of methane formation is given by the ratio of the rate of methane formation over the promoted Rh foil to the rate of methane

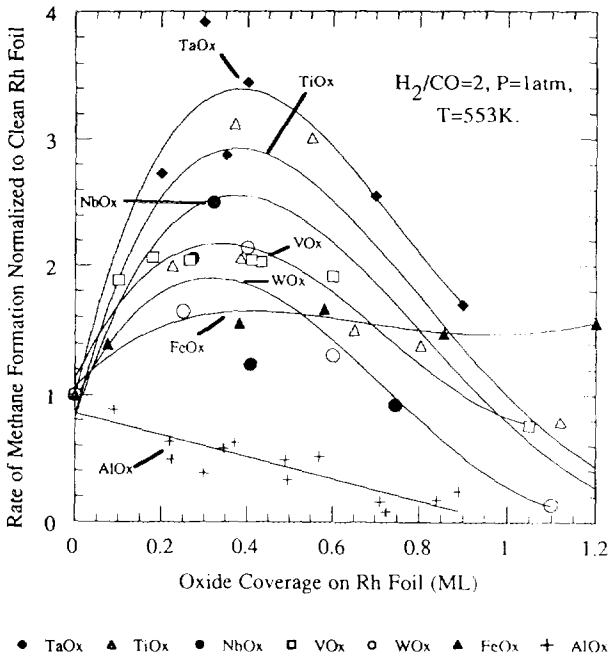

FIG. 1. Effect of metal oxide coverage on the rate of methane formation from CO and H_2 over Rh foil.

formation over the clean, unpromoted foil. For unpromoted Rh, the rate of methane formation is 0.034 s^{-1} for CO hydrogenation at 553 K in the presence of 253 Torr of CO and 506 Torr of H_2, and 0.19 s^{-1} for CO_2 hydrogenation at 523 K in the presence of 190 Torr of CO_2 and 570 Torr of H_2. The turnover frequencies measured for clean Rh foil are in good agreement with those reported previously for both Rh foil (27, 29) and Rh supported on SiO_2 and Al_2O_3 (30).

Figure 1 shows that with the exception of FeO_x and AlO_x, the relative rate of methane formation passes through a maximum near $\theta_{MO_x} = 0.4$ ml. It is noted that the rate of methanation does not go to zero as the metal oxide coverage goes to unity. This can be ascribed to the presence of residual exposed Rh due to the onset of three-dimensional growth of the oxide film for MO_x deposits of >0.9 ml. In the case of FeO_x promotion, the methanation rate rises but then reaches a plateau. For AlO_x deposits, the methanation rate decreases linearly. The overall ranking of the oxides by their effect on the rate of methanation from CO decreases in the order $TaO_x > TiO_x > NbO_x > VO_x > WO_x > FeO_x > AlO_x$.

With the exception of FeO_x, all of the metal oxides investigated enhance the rate of methane formation from CO_2 and Fig. 2 shows that the rate of methanation passes through a maximum with increasing metal oxide coverage. For FeO_x the methanation rate decreases linearly with decreasing oxide coverage. The extent of rate enhancement for CO_2 hydrogenation decreases in the order $TiO_x > NbO_x > TaO_x > ZrO_x > VO_x > WO_x > FeO_x$.

To determine the valence and stoichiometry of the metal oxides deposited on the Rh foil, XPS spectra of the surface were recorded both before and after CO and CO_2 hydrogenation. As an illustration, Ti 2p XPS spectra for a 0.5 ml deposit of titanium oxide are shown in Fig. 3. Spectra such as these were deconvoluted and the component peaks assigned to specific oxidation states of the metal based on a comparison of the binding energy for that peak with that for the metal in reference compounds (24, 31–82). The assignments of peak binding energies to specific oxidation states used in the present study are given in Table 1 along with assignments reported in the literature. For niobium oxide, the peak found at 204.7 eV lies between the literature assignments for NbO_2 and NbO and, hence, has been assigned to Nb^{3+}. For tantalum oxide the only known bulk phase is Ta_2O_5. However, in a study of the core binding energies of Group IIa, Vb, and VIb compounds, McGuire *et al.* (66) demonstrated a trend in the intrinsic chemical shifts of Nb, Ta, and W compounds. Therefore, based on the assignments for Nb, the peak in the Ta spectrum observed at 25.4 eV is assigned to Ta^{4+} and the peak observed at 24.3 eV is assigned to Ta^{3+}. The range of binding energies found in the literature for WO_2 is 32.5 to 34.4 eV. This range encompasses the peaks observed at 34.2 eV, 33.2 eV, and 32.5 eV. Since the peak at 33.2 eV exhibits the best agreement with the average value of the binding energy

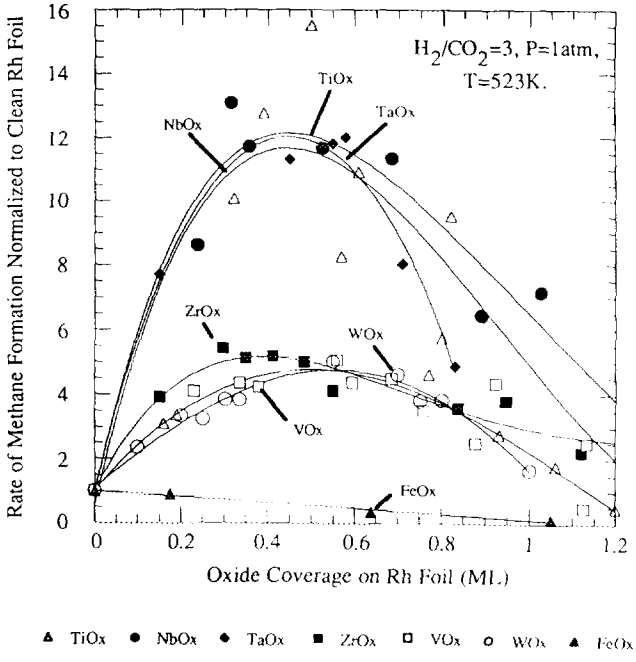

FIG. 2. Effect of metal oxide coverage on the rate of methane formation from CO_2 and H_2 over Rh foil.

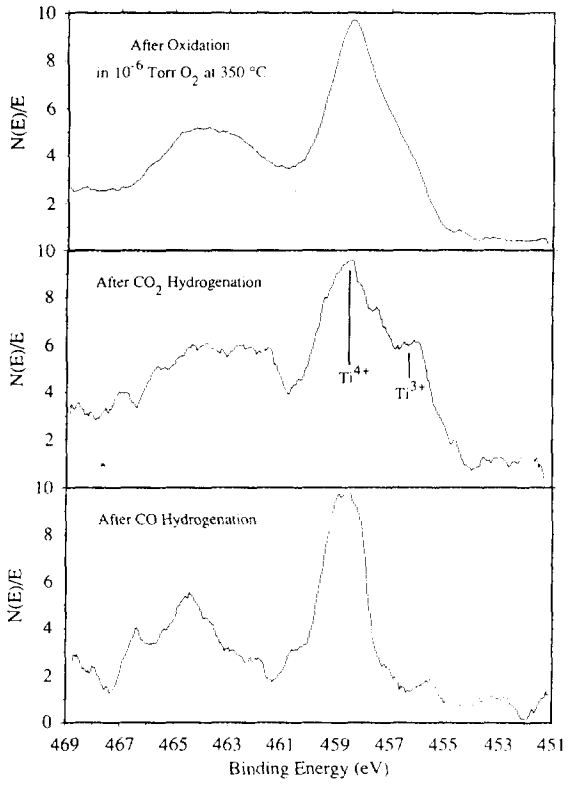

FIG. 3. XPS spectra of TiO_x and WO_x overlayers ($\theta_{MO_x} = 0.5$) deposited on a Rh foil. Spectra were taken after oxidation in O_2, after CO_2 hydrogenation, and after CO hydrogenation.

for W^{4+}, based on the literature, this peak is assigned to W^{4+}. The peak at 34.2 eV is then assigned to W^{5+} and that at 32.5 eV to W^{3+}. As an alternative, all three peaks could be assigned to W^{4+}; however, this would have little effect on the average oxidation state for W presented in Figs. 4 and 5. A more detailed presentation of the XPS results and the assignment of XPS peaks to specific oxidation states is given in Ref. (83).

Figure 4 shows the average oxidation state (Z) of the metal in the oxide overlayer following oxidation with 1×10^{-6} Torr O_2 for 5 min and that following CO hydrogenation at 553 K in the presence of 253 Torr CO and 506 Torr H_2. The average oxidation state is defined as the sum of the products of oxidation number times the fraction of the metal in that oxidation state. The oxides in Fig. 4 are arranged in the order of descending oxidation state measured after reaction. It is observed that after exposure to reaction conditions, the average oxidation state of TaO_x and NbO_x increases, the oxidation state of TiO_x and AlO_x is unchanged, and the oxidation state of VO_x, WO_x, and FeO_x decreases, relative to that observed following oxidation of the catalyst. The effect of CO_2 hydrogenation on the oxidation state of the metal in the oxide overlayer is given in Fig. 5. Here it is seen that only for ZrO_x is the oxidation state of Zr higher after reaction than after oxidation in O_2. For all of the other oxides the oxidation state of the metal is lower after reaction than after oxidation in O_2.

In the case of TiO_x, determinations of the oxidation state were made for a range of coverages. Figure 6 shows that the percentage of Ti in the 3+ oxidation state is higher following CO_2 than CO hydrogenation, but in both cases the percentage of titanium in the 3+ state decreases monotonically with increasing titania coverage.

Figure 7 illustrates the total amount of Ti^{3+} in the deposited TiO_x following the room-temperature adsorption of CO and subsequent temperature-programmed desorption to remove the oxygen present on the exposed Rh surface. Comparison of the Ti $2p^{3/2}$ XPS spectrum taken after CO titration with that taken after O_2 oxidation indicates that oxygen is removed from the TiO_x overlayer during CO titration. Figure 7 shows that the amount of Ti^{3+} (calculated as the product of the fraction of Ti present as Ti^{3+} times the coverage of TiO_x) observed after CO titration passes through a maximum for a TiO_x coverage of about 0.5 ML.

DISCUSSION

Deposition of submonolayer quantities of NbO_x, TaO_x, TiO_x, VO_x, WO_x, and ZrO_x on Rh causes an increase in the rate at which methane is formed via the hydrogenation of CO and CO_2. In each case, a maximum in the extent of enhancement relative to clean Rh foil is observed for a metal oxide coverage of about half a monolayer. These effects are qualitatively similar to those reported previously for TiO_x (23) and VO_x deposited on Rh foil (28) and for VO_x-promoted Rh/SiO_2 (7). As in the previous studies (26), the rate of methane formation from CO_2 is enhanced to a much greater degree than that for methane formation from CO.

The mechanisms for CO and CO_2 hydrogenation are similar (28). For both reactants the critical step is cleavage of the C–O bond in adsorbed CO or CH_xO ($x \leq 3$) species, the origin of adsorbed CO in the case of CO_2 hydrogenation being the dissociation of CO_2 (84–89). The C_s or $CH_{x,s}$ species released by C–O bond cleavage of CO or CH_xO readily undergoes hydrogenation to form CH_4. In support of this picture, it has been observed that adsorbed CO does not dissociate appreciably on Rh(111) surfaces (90) and that during temperature-programmed reduction of adsorbed CO by H_2, CH_4 and H_2O appear concurrently (7). Studies with Rh/SiO_2 indicate, as well, that the rate constant for CO dissociation is considerably smaller than that for CH_x hydrogenation (87).

The higher enhancement of methane formation from CO_2 than CO seen in Figs. 1 and 2 is consistent with the results previously reported for the effects of TiO_x (26) and

TABLE 1

Oxidation State Assignments

Oxide	This Work					Literature				
TiOx	4+	3+		ΔE^{4-3}		TiO_2 (4+)	Ti_2O_3 (3+)	TiO (2+)	ΔE^{4-3}	ΔE^{4-2}
	458.5	456.2		2.3		459.4[31,32], 459.2[33], 459.0[34], 458.9[35], 458.8[24,36,37], 458.7[38,40,41], 458.6-457.9[42,43], 458.5[44-48], 458.4[49,39]	457.5[34], 456.9[32], 456.8[44,47], 456.6[42], 456.5[43], 456.2[35], 455.7[24]	455.3[34], 455.0[43], 454.9[39], 454.8[47], 454.7[44], 454.6[46]	3.1[24], 2.7[35], 2.5[32], 2.1[43], 2.0[42], 1.7[44,47], 1.5[43]	3.9[46], 3.8[44], 3.7[34], 3.6[43], 50, 3.5[39]
ZrOx	4+	3+		ΔE^{4-3}		ZrO_2 (4+)	Zr_2O_3 (3+)		ΔE^{4-3}	
	182.3	181.1		1.2		183.3[51,52], 183.2-181.9[53], 182.9[54], 182.8[55], 182.5[56], 182.2[57,58,41,49], 181.9[58,59]	182.0[51], 181.7[55]		1.3[51], 1.1[55]	
FeOx	3+	2+	0	ΔE^{3-2}	ΔE^{3-0}	Fe_2O_3 (3+)	FeO (2+)	Fe (0)	ΔE^{3-2}	ΔE_{3-0}
	711.5	710.0	707.8	1.5	3.7	711.4[60], 711.2[61], 710.9[62], 710.7-710.3[63]	709.9[60], 709.7[61], 709.4[62]	707.7[60], 707.0[36,61]	1.5[60-62]	4.2[61], 3.7[60]
NbOx	5+	4+	3+	ΔE^{5-4}	ΔE^{5-3}	Nb_2O_5 (5+)	NbO_2 (4+)	NbO (2+)	ΔE^{5-4}	ΔE^{5-2}
	207.4	206.2	204.7	1.2	2.7	207.9[52], 207.8[64], 207.5[65,66], 207.4[67], 206.8[68]	207.3[52], 208.9[67], 205.3[69]	204.5[67], 203.7[69], 203.5[68], 202.8[65]	1.5[67,68], 0.6[52]	4.7[65], 3.9[68], 2.9[67]
TaOx	5+	4+	3+	ΔE^{5-4}	ΔE^{5-3}	Ta_2O_5 (5+)				
	26.3	25.4	24.3	0.9	2.0	26.8[66], 26.7[68,41], 26.2[52]				
VOx	+3	+2		ΔE^{3-2}		V_2O_5 (5+)	VO_2 (4+)	V_2O_3 (3+)	V(0)	ΔE^{5-3}
	515.6	513.8		1.6		518.1[70], 517.6[71,63,41,64,40,49], 517.4[36], 517.0[75], 516.7[72], 516.6[37,74]	517.4[70], 516.5[74], 516.1[75]	515.6[70], 515.5[75]	512.7[74], 512.4[73,76,77], 512.3[40], 512.2[36]	2.5[70], 1.5[75]
WOx	6+	5+	4+	3+	2+	WO_4 (6+)	WO_2 (4+)	W (0)	ΔE^{6-4}	
	35.4	34.2	33.2	32.5	31.9	36.8[66], 36.3-35.6[63], 36.0[78,79], 35.8[52,68,80], 35.5[81], 35.0[83]	34.4[78], 32.7[82], 32.5[81]	31.4[36]	3.0[81], 2.3[82], 1.6[78]	

VO_x (28). Williams *et al.* (27) have suggested that this effect might be due to the manner and degree to which the metal oxide affects the rate-limiting step in the reaction mechanism, and to differences in the surface coverage of the catalyst by atomic carbon and hydrogen, depending upon whether CO or CO_2 is the source of carbon. In the present study it was observed that after CO hydrogenation the C XPS signal intensity is threefold higher than that seen after CO_2 hydrogenation. The presence of a large amount of carbon on the surface could affect not only the rate of methane formation, but also the extent of metal oxide reduction and, hence, might explain why a less reduced metal oxide is observed after CO hydrogenation than after CO_2 hydrogenation.

It has been proposed that the effects of metal oxide promoters on the rate of methane formation from CO and CO_2 can be attributed to the formation of Lewis acid–base complexes between adsorbed CO or CH_xO at the boundary between the metal oxide and the exposed metal surface (1–5, 8, 17). The Lewis acid centers are envisioned to be the metal cations in the oxide located at the edge of the oxide overlayer. Access of CO adsorbed on the metal to these centers very likely requires the formation of anionic vacancies at the edge of the deposited oxide. Such Lewis acid–base interactions are envisioned to weaken the CO bond and facilitate its dissociation. In support of this it has been reported that the vibrational frequency of CO adsorbed on transition metals can decrease from the usual range of 2000 to 2100 cm^{-1} down to 1700–1600 cm^{-1} (5) in the presence of oxide promoters.

The observed maximal behavior of the extent of enhancement in the rate of methanation with oxide coverage seen in Figs. 1 and 2 is consistent with the idea that promotion by the oxide occurs only at the boundary between the oxide and the metal. AES characterization indicates that for submonolayer coverages, the oxide overlayer grows two-dimensionally, with only a small amount of three-dimensional growth being observed near the com-

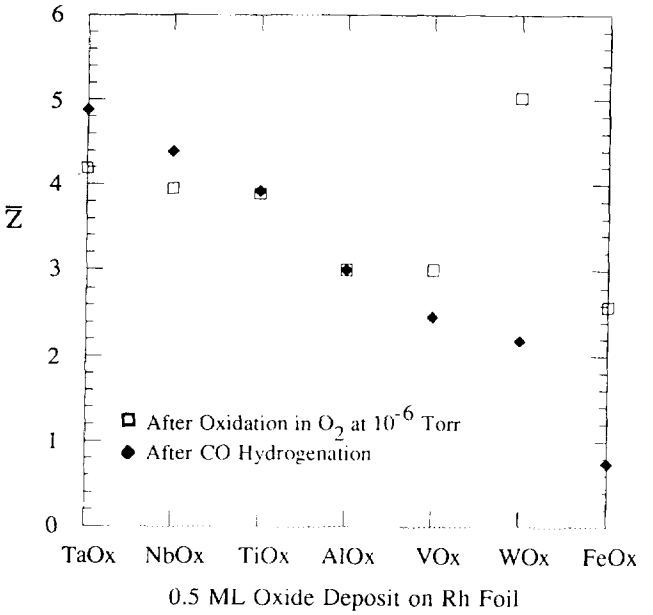

FIG. 4. Average oxidation state of the metal in the metal oxide overlayer measured after catalyst oxidation in O_2 and after CO hydrogenation.

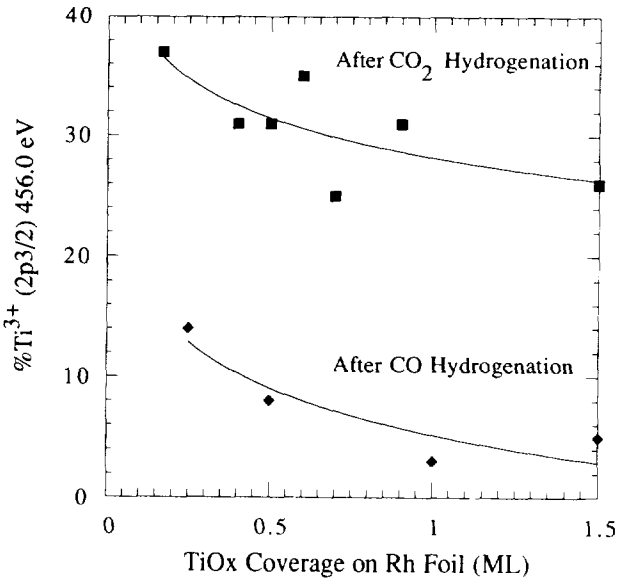

FIG. 6. Variation with TiO_x coverage of the percentage of Ti^{3+} in the overlayer following CO and CO_2 hydrogenation.

pletion of the first monolayer. Simulations of this mode of overlayer growth assuming a fixed number of nucleation sites leads to the conclusion that the concentration of sites along the metal–metal oxide boundary passes through a maximum at a coverage very near half a monolayer (91). The location of the maximum appears to be insensitive to the fraction of nucleation sites assumed, for nucleation fraction ranging from 0.1 to 10%. While direct observation of the morphology of the oxide deposit has not been feasible thus far, indirect evidence from XPS observations supports the picture of patchwise growth of the oxide layer. Boffa *et al.* (28) have reported that the

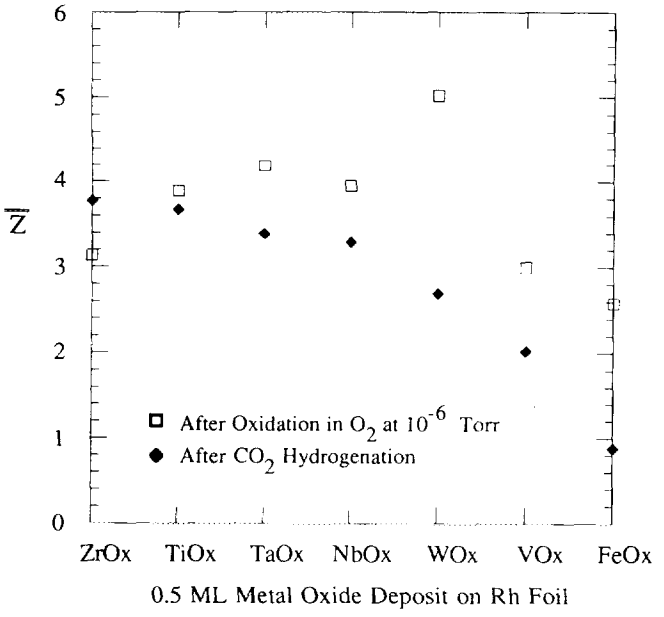

FIG. 5. Average oxidation state of the metal in the metal oxide overlayer measured after catalyst oxidation and after CO_2 hydrogenation.

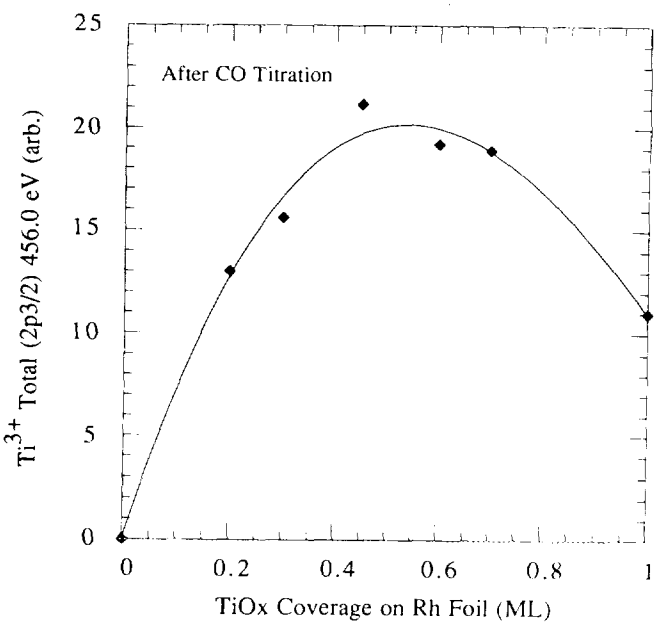

FIG. 7. Variation with TiO_x coverage of the amount of Ti^{3+} in the oxide overlayer following CO titration.

amount of cations in VO_x deposits present in the lower oxidation state (viz., V^{2+} versus V^{3+}) after CO titration of a fully oxidized surface passes through a maximum near half a monolayer as the oxide coverage is increased. A similar result is reported here in Fig. 7 for TiO_x. Since CO adsorption occurs only on the exposed metal surface and reduction of the oxide deposit can only occur by the reaction of adsorbed CO with the edge of the oxide deposit, the observed pattern in the proportion of metal cation in the lower oxidation state following CO titration is indicative of a patchy oxide overlayer.

The results presented in Figs. 1 and 2 demonstrate that the level of enhancement in the rates of methane formation from CO and CO_2 are a function of the metal oxide composition. Accepting the interpretation for the effects of metal oxide promoters presented above, the differences in the effectiveness of different oxides might be attributed to the strength of the Lewis acidity of the metal cations present in the oxide. If this hypothesis is correct the degree of rate enhancement should increase with increasing Lewis acidity of the oxide. Figures 8 and 9 show plots of the maximum degree of enhancement as a function of the Pauling electronegativity of the oxide cations, since Lewis acidity is proportional to the cation electronegativity (92, 93). The maximum rate of enhancement is taken from either Fig. 1 or 2 and the Pauling electronegativity is calculated from the expression

$$\chi_i = \chi_0(1 + 2Z), \qquad [1]$$

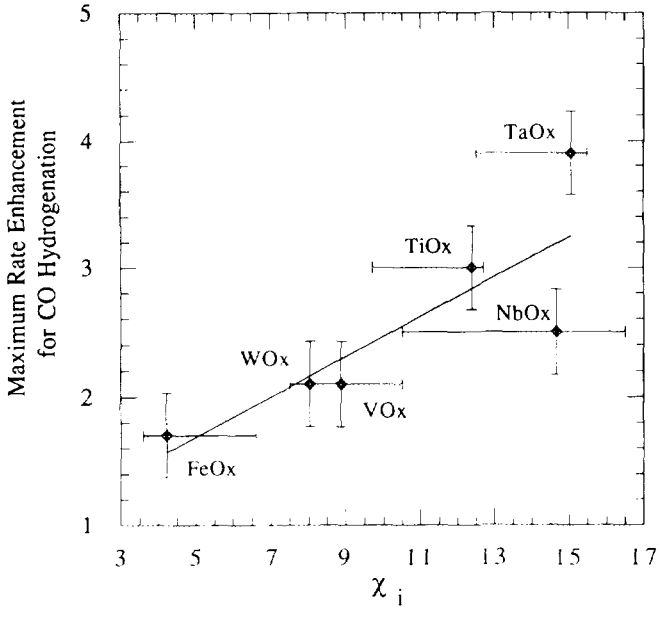

FIG. 8. Maximum enhancement in the rate of CO hydrogenation plotted as a function of the average electronegativity of the metal cation in the oxide.

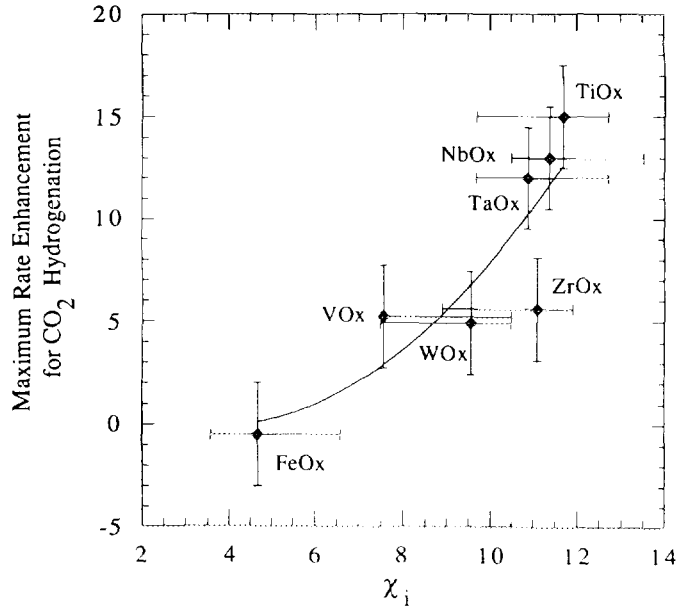

FIG. 9. Maximum enhancement in the rate of CO_2 hydrogenation plotted as a function of the average electronegativity of the metal cation in the oxide.

where χ_i is the electronegativity of the ion, χ_0 is the electronegativity of the element (Pauling scale), and Z is the oxidation state of the ion (94, 95). The "error" bars along the abscissa indicate the upper and lower limits of the electronegativity calculated for the lowest and highest oxidation states observed by XPS and the abscissa for each point is taken as the electronegativity for the average oxidation state observed under conditions of maximum rate enhancement. The error bars in the ordinate direction indicate the error associated with the measurement of the maximum degree of rate enhancement. The observed correlation between the degree of rate enhancement and the electronegativity of the oxide cation supports the hypothesis that Lewis acidity is the primary property determining the promoter effectiveness of an oxide originally proposed by Burch and Flambard (16) and later expanded by Sachtler and co-workers (8, 17). A further point to note is that the proposed interpretation nicely explains why the activity for CO hydrogenation over supported Rh increases in the following order of support composition $Nb_2O_5 > ZrO_2 > SiO_2 \approx Al_2O_3 > MgO$ (9, 10).

Since electronegativity depends on both the composition of the metal cation and its oxidation state, high levels of promotion should be expected for high values of χ_0 and Z. As demonstrated by the data presented in Figs. 4–6, the value of Z for a given oxide depends very strongly on reaction conditions. This suggests that the average oxidation state of the metal oxide is determined by the rates of oxidation and reduction of the oxide. One might

envision such redox cycles to comprise the following types of reactions,

$$MO_x + 2H_s = MO_{x-1} + H_2O$$
$$MO_x + CO_s = MO_{x-1} + CO_2,$$

where MO_x represents the oxidized form of the oxide and MO_{x-1} represents the partially reduced form of the oxide. In view of this, it is apparent that the effectiveness of an oxidic promoter depends on the reaction conditions, as well as the composition of the oxide prior to reaction.

Reference to Figs. 1 and 2 indicates that the effects of AlO_x on the rate of CO hydrogenation and the effects of FeO_x on the rate of CO_2 hydrogenation are distinctly different from those of all the other oxides examined. In both cases a linear decrease in the rate of methane formation is observed with increasing oxide coverage. The influence of AlO_x on the rate of CO hydrogenation is identical to that previously reported by Levin *et al.* (24). While the electronegativity of Al^{3+} lies between that of V^{3+} and Ti^{3+}, the Gibbs free energy for the reduction of AlO_x is significantly higher than that for VO_x or TiO_x. As a consequence, the formation of anionic vacancies in AlO_x should be considerably more difficult than in VO_x or TiO_x. Consistent with this, it is observed that the valence of Al atoms in AlO_x remains the same before and after reaction. As noted earlier, the formation of anionic vacancies is believed to be essential in order to provide access for the oxygen atom of adsorbed CO to the cations present at the perimeter of the oxide islands. Thus, while the electronegativity of Al^{3+} is sufficient for it to be an effective promoter of CO hydrogenation, the difficulty in forming anionic vacancies at the edge of AlO_x islands offsets this property. It should be noted, though, that the behavior of AlO_x on Pt is different from that on Rh. In the case of Pt, AlO_x has been reported to act as a promoter for CO hydrogenation (5).

While FeO_x is observed to inhibit the hydrogenation of CO_2 to methane, the reason for this effect is believed to be quite different from that discussed above for AlO_x. Figure 4 shows that under reaction conditions the average valence state of Fe in FeO_x is +1, implying that the oxide contains a mixture of Fe^0 and Fe^{2+}. The plot of maximum rate enhancement versus electronegativity presented in Fig. 8 indicates that the electronegativity of Fe in an average +1 valence state is too low for FeO_x to be a very effective promoter of CO_2 hydrogenation. However, inhibition of the reaction rate is not expected. It is conceivable that the metallic iron produced during reaction forms a surface alloy with Rh that for some reason is less active for CO_2 hydrogenation than pure Rh.

In closing this discussion, it is important to stress that the correlation between the enhancement in the rates of CO and CO_2 hydrogenation for different oxide promoters and the Pauling electronegativity (i.e., Lewis acidity) of the cations in the oxide, shown in Figs. 8 and 9, is based on the assumption that the metal oxide promotes the cleavage of the C–O bond in adsorbed CO or CH_xO through the formation of a Lewis acid-base adduct between metal cations exposed at the perimeter of the oxide and the O atom of the adsorbate. Implicit in this assumption is that the rate-limiting step in the formation of CH_4 involves cleavage of the C–O bond. It is recognized that enhancement in the rate of methane formation must depend on both the number of cation sites present at the perimeter of the oxide patches and the specific activity of each site, and that both of these quantities depend on the composition and structure of oxide.

While the results presented here support the hypothesis that the enhancement in the rates of CO and CO_2 hydrogenation is due to the presence of Lewis acid sites at the perimeter of the oxide patches, additional work is needed to confirm this picture more fully. In particular, the number of cationic sites exposed at the perimeter of the oxide patches deposited on Rh should be determined as a function of oxide composition, oxide coverage, and reaction conditions. Measurements should also be made of the rate coefficient for the rate-limiting step, so that the effects of oxide composition and oxidation state on the preexponential factor and the activation energy can be established.

CONCLUSIONS

Submonolayer quantities of oxides deposited on the surface of a Rh foil have a strong promoter effect on the hydrogenation of CO and CO_2. The effectiveness of different metal oxides increases with the oxidation state of the metal under reaction conditions. For a given metal oxide, the maximum increase in the rate of methane formation from either CO or CO_2 occurs at an oxide coverage of approximately half a monolayer. The enhancement in methanation rate is attributed to the formation of a Lewis acid-base complex between the oxygen end of adsorbed CO (or H_2CO) with exposed metal cations of the oxide located at the boundary between the oxide and Rh. This interaction is thought to weaken the C=O bond thereby facilitating either its cleavage or hydrogenation. The higher effectiveness of metal oxides in which the metal is in a high oxidation state is attributed to the higher Lewis acidity of the oxide. The oxidation state of the metal in a given oxide is noticeably lower during CO_2 hydrogenation than CO hydrogenation. This pattern is ascribed to the higher surface concentration of hydrogen on the Rh surface during CO_2 hydrogenation.

ACKNOWLEDGMENT

This work was supported by the Director, Office of Energy Research, Office of Basic Energy Sciences, Materials Sciences Division of the U.S. Department of Energy under Contract DE-AC03-SF00098.

REFERENCES

1. Tauster, S. J., *Acct. Chem. Res.* **20,** 389 (1987).
2. Bell, A. T., *in* "Catalyst Design—Progress and Perspectives" (L. L. Hegedus, Ed.), Wiley, New York, 1987.
3. Burch, R., *in* "Hydrogen Effects in Catalysis" (Z. Paal and P. G. Menon, Eds.), Dekker, New York, 1988.
4. Haller, G. L., and Resasco, D. E., *Adv. Catal.* **36,** 173 (1989).
5. Vannice, M., A., *Catal. Today* **12,** 255 (1992).
6. Mochida, I., Nobuhide, I., Ishibashi, H., and Fujitsu, H., *J. Catal.* **110,** 159 (1988).
7. Koerts, T., Welters, W. J. J., and van Santen, R. A., *J. Catal.* **134,** 1 (1992).
8. Sachtler, W. M. H., and Ichikawa, M., *J. Phys. Chem.* **90,** 4752 (1986).
9. Iizuka, T., Tanaka, Y., and Tanabe, K., *J. Catal.* **76,** 1 (1982).
10. Iizuka, T., Tanaka, Y., and Tanabe, K., *J. Mol. Catal.* **17,** 381 (1982).
11. Trovarelli, A., Mustazza, C., Dolcetti, G., Kaspar, J., and Graziani, M., *Appl. Catal.* **65,** 129 (1990).
12. Johnston, P., Joyner, R. W., Pudney, P. D. A., Shapiro, E. S., and Williams, B. P., *Faraday Discuss. Chem. Soc.* **89,** 91 (1990).
13. Hindermann, J. P., Kiennemann, A., and Tazkritt, S., *in* "Structure and Reactivity of Surfaces" (C. Morterra, A. Zecchina, and G. Costa, Eds.), Elsevier, Amsterdam, 1989.
14. Schwab, G.-M., *Adv. Catal.* **27,** 1 (1978).
15. Solymosi, F., *Catal. Rev.* **1,** 233 (1967).
16. Burch, R., and Flambard, A. R., *J. Catal.* **86,** 384 (1982).
17. Sachtler, W. M. H., Shriver, D. F., Hollenberg, W. B., and Lang, A. F., *J. Catal.* **92,** 429 (1985).
18. Chung, Y.-W., Xiong, G., and Kao, C. C., *J. Catal.* **85,** 237 (1984).
19. Demmin, R. A., Ko, C. S., and Gorte, R. J., *J. Phys. Chem.* **89,** 1151 (1985).
20. Demmin, R. A., and Gorte, R. J., *J. Catal.* **98,** 577 (1986).
21. Demmin, R. A., and Gorte, R. J., *J. Catal.* **105,** 373 (1987).
22. Levin, M. E., Salmeron, M., Bell, A. T., and Somorjai, G. A., *Surf. Sci.* **169,** 123 (1986).
23. Levin, M. E., Salmeron, M., Bell, A. T., and Somorjai, G. A., *J. Catal.* **106,** 401 (1987).
24. Levin, M. E., Salmeron, M., Bell, A. T., and Somorjai, G. A., *Surf. Sci.* **195,** 429 (1988).
25. Williams, K. J., Salmeron, M., Bell, A. T., and Somorjai, G. A., *Surf. Sci.* **204,** L745 (1988).
26. Williams, K. J., Boffa, A. B., Salmeron, M., Bell, A. T., and Somorjai, G. A., *Catal. Lett.* **5,** 385 (1990).
27. Williams, K. J., Boffa, A. B., Salmeron, M., Bell, A. T., and Somorjai, G. A., *Catal. Lett.* **9,** 41 (1991).
28. Boffa, A. B., Bell, A. T., and Somorjai, G. A., *J. Catal.* **139,** 602 (1993).
29. Sexton, B. A., Hughes, A. E., and Foger, K., *J. Catal.* **77,** 895 (1982).
30. Solymosi, F., Erlohelyi, A., and Bansagi, T., *J. Catal.* **68,** 371 (1981).
31. Rao, K. N., Mohan, S., Hegde, M. S., and Balasubramanian, T. V., *J. Vac. Sci. Technol. A* **11,** 394 (1993).
32. Paul, J., Cameron, S. D., Dwyer, D. J., and Hoffmann, F. M., *Surf. Sci.* **177,** 121 (1986).
33. Murata, M., Wakino, K., and Ikeda, S., *J. Electron Spectrosc. Relat. Phenom.* **6,** 459 (1975).
34. Carley, A. F., Chalker, P. R., Riviere, J. C., and Roberts, M. W., *J. Chem. Soc., Faraday Trans. 1* **83,** 35 (1987).
35. Greenlief, C. M., White, J. M., Ko, C. S., and Gorte, R. J., *J. Phys. Chem.* **89,** 5025 (1985).
36. Moulder, J. F., Stickle, W. F., Sobol, P. E., and Bomben, K. D., *in* "Handbook of X-Ray Photoelectron Spectroscopy," 2nd ed., Perkin-Elmer Co., Physical Electronics Division, Eden Prairie, MN, 1992.
37. Zhao, L. Z., Liu, S. H., Wang, D. H., and Pan, C. H., *J. Electron Spectrosc. Relat. Phenom.* **52,** 571 (1990).
38. Fung, S. C., *J. Catal.* **76,** 225 (1982).
39. Simon, D., Perrin, C., and Bardolle, J., *J. Microsc. Spectrosc. Electron* **1,** 175 (1976).
40. Wagner, C. D., Riggs, W. D., Davies, L. E., Moulder, J. F., and Mullenberg, G. E. *in* "Handbook of X-Ray Photoelectron Spectroscopy," Perkin-Elmer Co., Physical Electronics Division, Eden Prairie, MN, 1976.
41. Nefedov, V. E., Gati, D., Dzhurinskii, B. F., Sergushin, N. P., and Salyn, Y. V., *Zh. Neorg. Khim.* **20,** 2307 (1975).
42. Dwyer, D. J., Cameron, S. D., and Gland, J., *Surf. Sci.* **159,** 430 (1985).
43. Sheng, T., Gouxing, X., and Hongli, W., *J. Catal.* **111,** 136 (1988).
44. Kuznetsov, M. V., Zhuravlev, Ju. F., Zhilyaev, V. A., and Gubanov, V. A., *J. Electron Spectrosc. Relat. Phenom.* **58,** 1 (1992).
45. Espinos, J. P., Gonzalez-Elipe, A. R., and Munurea, G., *Appl. Surf. Sci.* **62,** 137 (1992).
46. Beard, B. C., and Ross, P. N., *J. Phys. Chem.* **90,** 6811 (1986).
47. Hofmann, S., and Sanz, J. M., *J. Trace Microprobe Tech.* **1,** 213 (1982–83).
48. Munuera, G., Gonzalez-Elipe, A. R., Espinos, J. P., Conesa, J. C., Soria, J., and Sanz, J., *J. Phys. Chem.* **91,** 6625 (1987).
49. Nefdov, V. I., Salyn, Y. V., Chertkov, A. A., and Padurets, L. N., *Zh. Neorg. Khim.* **19,** 1443 (1974).
50. Pan, J. M., Diebold, U., Zhang, L., and Madey, T. E., *Surf. Sci.* **295,** 411 (1993).
51. Kumar, L., Sarma, D. D., and Krummacher, S., *Appl. Surf. Sci.* **32,** 309 (1988).
52. Sarma, D. D., and Rao, C. N. R., *J. Electron Spectrosc. Relat. Phenom.* **20,** 25 (1980).
53. Harel, S., Mariot, J. M., and Hague, C. F., *Surf. Sci.* **269/270,** 1167 (1992).
54. De Gonzalez, C. O., and Garcia, E. A., *Surf. Sci.* **193,** 305 (1988).
55. Morant, C., Sanz, J. M., Galan, L., Soriano, L., and Rueda, F., *Surf. Sci.* **218,** 331 (1989).
56. Huang, N. K., Kheyrandish, H., and Colligon, J. S., *Mater. Res. Bull.* **27,** 239 (1992).
57. Barr, T. L., *J. Phys. Chem.* **82,** 1801 (1978).
58. Barr, T. L., *J. Vac. Sci. Technol.* **14,** 660 (1977).
59. Majumdar, D., and Chatterjee, J., *Appl. Phys.* **70,** 988 (1991).
60. Kurtz, R. L., and Henrich, V. E., *Surf. Sci.* **129,** 345 (1983).
61. Brundle, C. R., Chuang, T. J., and Wandelt, K., *Surf. Sci.* **68,** 459 (1977).
62. McIntyre, N. S., and Zetaruk, D. G., *Anal. Chem.* **49,** 1521 (1977).
63. Nefedov, V. I., Salyn, Y. V., Leonhardt, G., and Scheibe, R., *J. Electron Spectrosc. Relat. Phenom.* **10,** 121 (1977).
64. Nefedov, V. I., Firsov, M. N., and Shaplygin, I. S., *J. Electron Spectrosc. Relat. Phenom.* **26,** 65 (1982).
65. Simon, D., Perrin, C., and Baillif, P. C., *R. Acad. Sci. Ser. C* **283,** 241 (1976).
66. McGuire, G. E., Schweitzer, G. K. K., and Carlson, T. A., *Inorg. Chem.* **12,** 2451 (1973).
67. Fountaine, R., Caillat, R., Feve, L., and Guittet, M. J., *J. Electron Spectrosc. Relat. Phenom.* **10,** 349 (1977).

68. Shelef, M., Haack, L. P., Soltis, R. E., DeVries, J. E., and Logothetis, E. M., *J. Catal.* **137,** 114 (1992).
69. Bahl, M. K., *J. Phys. Chem. Solids* **36,** 485 (1975).
70. Nag, N. K., Massoth, F. E., *J. Catal.* **124,** 127 (1990).
71. Hamrin, K., Nordling, C., and Kihlborg, L., *Ann. Acad. Regiae Sci. Ups.* **14,** 70 (1970).
72. Gil-Llambias, F. J., Escudey, A. M., Fierro, J. L. G., and Lopez Agudo, A., *J. Catal.* **95,** 520 (1985).
73. Larsson, R., Folkesson, B., and Schon, G., *Chem. Scr.* **3,** 88 (1973).
74. Kasperkiewicz, J., Kovacich, J. A., and Lichtman, D., *J. Electron Spectrosc. Relat. Phenom.* **32,** 123 (1983).
75. Colton, R. J., Guzman, A. M., and Rabalais, J. W., *J. Appl. Phys.* **49,** 409 (1978).
76. Romand, M., Roubin, M., *Anausis* **4,** 309 (1976).
77. Shul'ga, Y. M., Troitskii, V. N., Aivazov, M. I., and Borod'ko, Y. G., *Zh. Neorg. Khim.* **21,** 2621 (1976).
78. Biloen, P., and Pott, G. T., *J. Catal.* **30,** 169 (1973).
79. Kerkhof, F. P. J. M., and Moulijn, J. A., *J. Electron Spectrosc. Relat. Phenom.* **14,** 453 (1973).
80. Walter, J. L., and Lou, K. A., *J. Mater. Sci.* **24,** 3577 (1989).
81. Ng, K. T., and Hercules, D. M., *J. Phys. Chem.* **80,** 2094 (1976).
82. Colton, R. J., Rabalais, J. W., *Inorg. Chem.* **15,** 237 (1976).
83. Boffa, A. B., Ph.D. Thesis, Department of Chemistry, University of California, Berkeley, CA, 1994.
84. Henderson, M. A., and Worley, S. D., *J. Phys. Chem.* **89,** 1417 (1985).
85. Rieck, J. S., and Bell, A. T., *J. Catal.* **96,** 88 (1985).
86. Shustorovich, E., and Bell, A. T., *J. Catal.* **113,** 341 (1988).
87. Mori, T., Masuda, H., Imai, H., Miyamoto, A., Hasebec, R., and Murakami, Y., *J. Phys. Chem.* **87,** 3648 (1983).
88. Mori, T., Miyamoto, A., Niizuma, H., Takahashi, N., Hattori, T., and Murakami, Y., *J. Phys. Chem.* **90,** 109 (1986).
89. Mori, T., Miyamoto, A., Niizuma, H., Takahashi, N., Hattori, T., and Murakami, Y., *J. Phys. Chem.* **93,** 2039 (1986).
90. Castner, D. G., Sexton, B. A., and Somorjai, G. A., *Surf. Sci.* **71,** 519 (1978).
91. Williams, K., Ph.D. Thesis, Department of Chemical Engineering, University of California, Berkeley, CA, 1990.
92. Tanabe, K., "Solid Acids and Bases," Kondansha, Tokyo/Academic Press, New York, 1970.
93. Tanabe, K., *in* "Catalysis—Science and Technology" (M. Boudart and J. Anderson, Eds.), Vol. 2 Springer-Verlag, Berlin, 1981.
94. Tanaka, K. I., and Ozaki, A., *J. Catal.* **8,** 1 (1967).
95. Sanderson, R. T., *in* "Chemical Periodicity," Reinhold, New York, 1960.